Quantifying risk of ground impact fatalities of power line inspection BVLOS flight with small unmanned aircraft

La Cour-Harbo, Anders

Published in:
2017 International Conference on Unmanned Aircraft Systems (ICUAS)

DOI (link to publication from Publisher):
10.1109/ICUAS.2017.7991323

Publication date:
2017

Document Version
Early version, also known as pre-print

Quantifying risk of ground impact fatalities of power line inspection BVLOS flight with small unmanned aircraft

Anders la Cour-Harbo[1]

Abstract— **One of the major challenges of conducting operation of unmanned aircraft, especially operations beyond visual line-of-sight (BVLOS), is to make a realistic and effective risk assessment. An important part of such an assessment is to identify the risk of fatalities, preferably in a quantitative way since this allows for comparison with manned aviation to determine whether an equivalent level of safety is achievable. This works presents a method for quantifying the probability of fatalities resulting from an uncontrolled descent of an unmanned aircraft conducting a BVLOS flight. The method is based on a standard stochastic model, and employs parameterized high fidelity ground impact distribution models that accounts for both aircraft specifications, parameter uncertainties, and wind. The method also samples the flight path to create an almost continuous quantification of the risk as a function of mission flight time. The probability of fatality is determined for a Talon model aircraft on a power line inspection mission.**

I. INTRODUCTION

A. Background

As part of the regulatory process in Denmark the Danish Transport, Construction and Housing Authority decided in early 2016 to initiate a project called BVLOS FastTrack to investigate what requirements and circumstances would be appropriate in order to grant (initially) a few companies permission to routinely conduct BVLOS operations in Danish airspace. At that time no permissions had been granted for BVLOS flight in Denmark expect for flights in Greenland and individual flights confined to specific routes and dates. The purpose of the project was to grant permissions based on a thorough and scientific analysis of the risks involved for a type of flight rather than just one specific flight. Danish UAS operator companies were invited to participate in the project, and their contribution would be supplying all information required for a thorough analysis as well as conducting a number of test flights to demonstrate the ability to adhere to proper procedures. In turn they would be, should the risk of their proposed BVLOS flight be acceptable, granted permission to conduct BVLOS operations within given limitations. The incitement would be that these limitation would not be specifically geographical and temporal, meaning that a flight permission would state that any flight within the given limits would be permitted independent of geographical location and point in time.

A few companies participated in the project with rather different applications for the flights. This work focuses on Heliscope, a Danish UAS inspection company that uses unmanned aircraft for powerline inspections, and presents how we developed risk profile for their particular type of flight. The aim of this work as well as the BVLOS FastTrack project is to develop a method that allows for immediate quantification of the risk for people on the ground when a given unmanned aircraft flies overhead.

[1]Aalborg University, Dept. of Electronic Systems, Fredrik Bajers Vej 7C, 9220 Aalborg East, Denmark

B. Previous work

There are numerous works on how to conceptually approach the challenge of determining the risk of an unmanned aircraft flight. Much is borrowed from the world of manned aviation that has been conducting risk management for decades. A number of examples of risk assessments and quantifications for unmanned aircraft are the following. [1] addresses the lack of an accepted framework and provides some guidelines for how to apply existing models to manage the risk. In [2] a comprehensive description of how to manage the risk of unmanned aircraft operations, including 'the systematic application of management policies, procedures and practices to the activities of communicating, consulting, establishing the context, and assessing, evaluating, treating, monitoring and reviewing risk.' This work also presents a series of quantification of existing risks for various types of aviation. Metrics for safety, including hazard metrics and risks metrics are presented in [3], in [4] a software safety case is developed, and in [5] a generic safety case is presented based on experience with NASA unmanned aircraft missions.

The uncontrolled descent of unmanned aircraft into populated areas have been the subject in a number of publications. This includes [6] that investigate larger aircraft through an equivalent level of safety analysis. [7] specifically looks at distribution of possible impact locations based on simulation, and [8] uses the standard statistical setup (which is also used in this work) and applies a normal distribution approach using aircraft glide parameters to model the impact location. The barrier bow tie model also used in manned aviation risk assessment is presented in [9].

C. Current work

The aim in this work is to go beyond a qualitative approach that provides framework for risk assessment, and instead use a quantitative approach to determine as accurately as possible, the level of safety for a given flight operation, using a metric similar to what is used in manned aviation, i.e. fatalities per flight hour. The modelling of the probability of fatalities is done with a stochastic approach similar to many of the previous works listed above. However, the determination of the individual probabilities in the model is

done using georeferenced probability density functions at a high fidelity and (almost) continuously along the flight path to provide not just a single probability for the entire flight, but indeed a fatality rate for the flight path itself. The details of the stochastic modelling of impact areas for uncontrolled descents is beyond the scope of this work, and is provided in separate publications by this author, see [10] and [11].

II. METHODS

The basic approach is similar to previous work in using a stochastic model that joins probabilities in the causal chain from drone malfunction to a potential fatality. The specific design of this stochastic model varies from work to work; here, in Section II-A, we use a fairly simple setup, where the focus is on the probabilities related to the aircraft ground/person impact. The model is used for three different types of flight terminating events, see Section II-B, each with their own high resolution ground impact probability density function, see Section II-C, including the effect of wind, see Section II-D and associated event probability, see Section II-E. Rather than a priori assuming an average population density for the entire flight (as seen in most previous work), we employ a high resolution population density map, see Section II-F. Finally, a map from person impact to probability of fatality is used, based on work in the field of forensic science, see Section II-G.

We then use the stochastic model on a (sufficiently densely) sampled flight path to determine the probabilities of fatality as a function of the flight path, and subsequently determine the total flight risk by summing over the flight path. This is done separately for the different types of flight terminating events to accommodate the varying lethality parameters associated with the manner in which the aircraft descents in each of the event scenarios. The is described in more detail along with the results in Section III.

A. Probability of fatality

For computing the probability of fatality we will use this standard formulation similar to what is employed in several of the previous works listed in Section I-B.

$$p_{\text{fatality}} = p_{\text{event}} \cdot p_{\text{impact person}} \cdot p_{\text{fatal impact}} , \quad (1)$$

where p_{event} is the probability per hour of a given event (of which we will use three), $p_{\text{impact person}}$ is the conditional probability that given an occurrence of one of the events that a person will be impacted, and $p_{\text{fatal impact}}$ is the conditional probability, given a person is impact as a result of one of the event, that this person suffers a fatal injury.

We will include three events; ballistic decent, uncontrolled glide, and fly-away (see II-B). We will attach a given probability to each of these based primarily on the work of others (see section II-E).

The probability of impacting a person is computed by establishing a georeferenced probability density function for each type of event associated with the geographical location where the event happens, correlating this with a population density map of sufficient resolution, and modifying the result to account for various factors pertaining to each event type. The result is a probability of impacting a person should each of the events happen at the specified geographical location, and will thus be dependent on the actual flight path of the aircraft.

B. Crash events

For this particular mission flown by the Heliscope Talon aircraft we use three different events that can occur during flight and will force a descent of the aircraft in a manner that does not allow for reaching either home or any designated safe impact zone. These are

1) **Ballistic descent** This is a situation where the aircraft looses most of its lift, for instance by a wing breaking off or loosing a motor (physically separating from the aircraft). The aircraft will then enter a (close to) ballistic descent governed mainly by the drag of the crippled aircraft and the wind.
2) **Uncontrolled glide** This is total loss of power on a fixed wing aircraft, meaning loss of thrust and control authority. The airframe is intact. The aircraft is assumed to enter a glide path governed by the glide ratio and the wind. The deflection surface are assumed to be in a close to neutral position that may lead to a slightly 'curved' glide.
3) **Fly-away** This is loss of control authority of the aircraft, while it continuous to operate as a powered aircraft. The motion of the aircraft is controlled by the autopilot, and it may fly to its maximum range in any direction, including vertically up.

It is quite easy to envision and include additional failure scenarios such as a spin due to a stuck actuator, loss of a vital sensor that leaves the aircraft without useful navigation, a vertical descent of a quad rotor due to loss of thrush on one arm, and so on.

It is assumed that the failure event happens at some point during the flight and that the resulting impact point on the ground is relative to this point of failure. The ground impact point is modelled with the uncertainties that reasonably may affect the descent, for instance that the drag coefficient of a aircraft without the wing is not known precisely. Additionally, the ballistic and uncontrolled glide events also include the effect of wind (with appropriate stochastic assumptions on speed and direction). The details of modelling the ballistic descent is present in [10] and the details of the uncontrolled glide and fly-away are present in [11].

C. Modelling of ground impact probability density function

The ballistic descent is modelled with a second order dependance on speed and under influence of gravity g. The flight speed is v and initial (prior to event) flight velocity is orthogonal to gravity. For a no-wind scenario this gives a travelled distance in flight velocity direction of

$$x(y) \approx \frac{m}{c} \ln\Big(1 + \frac{v\sqrt{c}(m \ln 2 + cy)}{m\sqrt{mg}}\Big), \quad cy > m \quad (2)$$

for a given altitude y, where m is the aircraft mass, and $c = \frac{1}{2}\rho A C_{\mathrm{D}}$ with ρ is the air density, A is the frontal area creating drag, and C_{D} the drag coefficient. The approximation is quite good for $cy > m$, which is the case for the Talon aircraft at operational altitude. The drag coefficient and the flight speed are both stochastic variables assumed to be normally distributed. The probability density function for x then gives the probability of reaching a given distance during a ballistic descent.

The uncontrolled glide assumes the aircraft is descending as a glider, that is unpropelled and in an aerodynamic equilibrium configuration with actuators in neutral or close to neutral positions (no banking with ailerons and no turning with the rudder). The glide ratio γ, the horizontally travelled distance per vertically descended distance, is given as a stochastic variable with mean equal to the estimated glide ratio and a variance to accommodate for variations in elevator deflection angle and variation in drag due to possible modifications of the aircraft to accommodate missions sensors. The distance travelled in an uncontrolled glide is thus $x(y) = \gamma y$.

A fly-away is assumed to be able to take the aircraft as far as the maximum range (subject to the amount of 'fuel' left), and all compass directions are equally probable. The probability of ground impact is assumed to decreases linearly with distance to the event point, reaching zero at maximum range. Thus, the probability density function becomes a right circular cone with apex at the event point and base coinciding with the ground surface.

D. Wind

The influence of wind is significant for the unpropelled events, ballistic descent and uncontrolled glide, as it will cause the aircraft to be transported a given distance in the wind direction. The actual distances travelled is assumed to be equal to the wind velocity times the time it takes the aircraft to descent from flight altitude to the ground. For the ballistic descent this time is given as

$$t(y) \approx \frac{m \ln 2 + cy}{\sqrt{cmg}} \tag{3}$$

under the same conditions as (2), and for the uncontrolled glide it will be $t(y) = \gamma y / v_{\mathrm{glide}}$, where v_{glide} is the horizontal glide speed, assumed to be not too different from the flight speed. The wind direction is assumed to be uniformly distributed in all directions, and the wind velocity is assumed to be normally distributed with a given mean and variance. The effect of this is that the PDFs for the ground impact point becomes two dimensional for both events. An example of a PDF for a ballistic descent in shown in Figure 2 (the example is taken from [10], where additional examples for non-uniformly distributed wind direction are also presented).

E. Probability of events

The events that renders the aircraft uncontrollable and eventually lead to a descent each has a probability attached to them. For the computations in this work we simply assume a certain value measured in 'per flight hour'. For instance the probability of a ballistic descent is set to 1/50 per flight hour. The probabilities used are rough estimates based on the works of others (see below) as well as the experience of the BVLOS FastTrack project team. The event probability enters the total probability computation in (1) as a scalar, and consequently the effect of changing the event probability is a simple scaling.

The probability of a flight terminating malfunction on an unmanned aircraft has been studied by a number of groups. A reliability assessment of an Ultra Stick 120 is made in [12] and [13] using failure mode effect and analysis (FMEA), with particular attention to the control surfaces and servos. No specific probabilities are provided, but are considered to be high. In [14] probabilities related to military unmanned aircraft are reported, and the probability of a flight terminating event is in the order of 10^{-4} – 10^{-2} per flight hour, with the probability for smaller aircraft being somewhat higher that for the larger aircraft. A group of students showed in [15] using FMEA based on component failure rates that their Ultra Stick 120 has on average 2.17 catastrophic (flight terminating) failures per 100 flight hours. The type of failures considered relates to the ballistic descent and uncontrolled glide in the present work. In [16] they showed how a dedicated reconstruction of the aircraft based on a fault tree analysis could theoretically reduce the failure rate by 20 times, and they were able to implement changes to the physical aircraft to achieve a catastrophic failure rate of 0.76 per 100 flight hours. Actuators and control surfaces are investigated in [17], [18] where the probability of an uncontrollable aircraft is modelled assuming a servo fault detection algorithm. In [19] a method for estimating mechanical failure rate of small unmanned aircraft is presented, and an example is provided based on the SPAARO aircraft at 25 kg. The example explicitly lists the used probabilities for servo and deflection surfaces as well as engine and battery, and these probabilities are provided by two experiences RC pilots. Probabilities of failure for a wing bolt and main spar are theoretically derived. The resulting failure rate for the aircraft (covering the ballistic and uncontrolled glide events) is 0.19 failures per flight hour. With suggested improvements for the engine, wing bolt, servos, and redundant control surfaces the failure can be reduced to 0.028 failure per flight hours (equivalent to 36 hours between failures). Note that this includes non-catastrophic failures, where the aircraft may be able to return home.

The Heliscope Talon aircraft is specifically used for BVLOS flights and reliability is therefore a primary concern. This means that alterations made to the aircraft as well as the maintenance and operational procedures are focused on providing a reasonably reliable aircraft. Combined with the figures referenced above from literature, the probabilities listed in Table I seems probable, without being neither conservative nor optimistic. As the aircraft accumulates flight hours these probabilities can be updated to more accurately reflect the true probabilities for that aircraft.

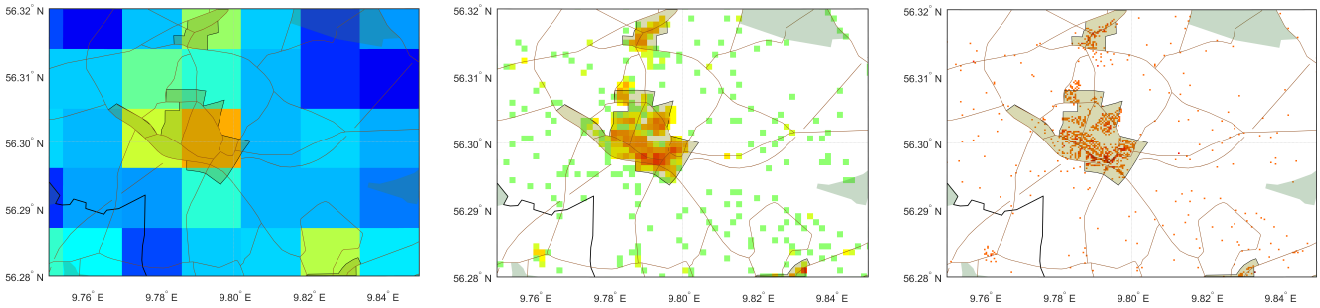

Fig. 1. From left to right people density maps with resolutions of 1 km, 100 m, and 25 m. The color scale is the same and goes from 0 (white) through 1 (dark blue) to 40.000 person/km^2 (dark red). Note how the density tends to grow with increased resolution due to the same number of people being registered in still smaller squares. Semi-transparent topographical information is overlaid; roads are brown, urban areas in dark yellow, forest in green, and municipality border in black. The town in the center of view is Thorsø.

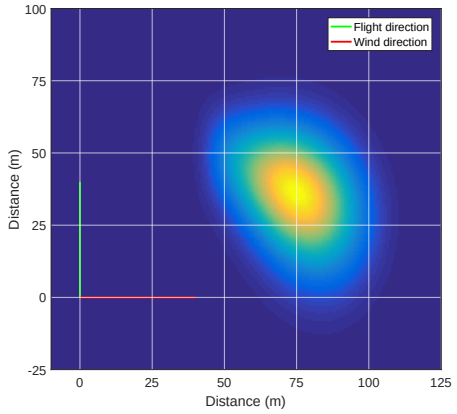

Fig. 2. An example of a PDF for a ballistic event with altitude $y = 150$, aircraft mass $m = 2$, front area of 0.1 m^2, $C_\mathrm{D} \sim N(\mu = 0.9, \sigma = 0.2)$, speed $v \sim N(15, 1)$, wind compass heading $N(90, 2)$ (east), wind speed $N(12, 8)$, and flight direction is compass heading 0 (north). Dark blue is zero probability and yellow is highest probability. The PDF resolution is 1 m by 1 m.

F. People density

The density of people on the ground is the main factor in the probability of impacting a person in the event of a crash. For the BVLOS flights where long distances are typically covered the variation in people density can be significant during the flight. Also, the different type of descent varies somewhat in impact area (that is, a ballistic descent is typically close to the incident location, whereas a flyaway may lead to a descent many kilometers from the incident location). This means that for some events the resolution of the people density map must be fairly high to give accurate estimates of the person impact probability, while for other events the resolution can be more coarse and still give accurate results.

A list of geographical coordinates of all addresses in Denmark is publicly available and we have used this to generate people density maps with varying resolution to fit the different types of descent. While a fine resolution will of course work for any type of event the computation time grows significantly, so maps are generated that suits the spatial extend of the impact area for each type of event. In figure 1 are shown three examples of such maps.

While these maps does show where people live they obviously do not show where people actually are. As this information is evidently very difficult to obtain we will make the assumptions that people are, with some probability, in the vicinity of their home, and are outside exposed to a small unmanned aircraft potentially descending. Inspired by [20] an appropriate probability of people being exposed is around 30%. This is also referred to as the shelter factor. We will also assume that the number of people associated with each address is equal to the average number of people in a Danish household. This number is 5.75M people divided by 2.65M households, equal to 2.17 people per household. The number of addresses is 3.3M as some addresses are not households, but rather businesses and industry. The density map used in this work is no adjusted to account for this.

G. Probability of fatality when impacted

When a drone impacts a human there is a probability that the impact will inflect injuries that will result in a fatality. Determining this probability for a given person and a given drone is not simple, partly because of the many different ways the impact can occur, and partly because the easily determined parameters, such a speed and mass, do not have a simple correlation to injury severity, because the human body reacts differently depending on the impacted body part, and the fact that injuries primarily relate to how fast and where the kinetic energy is dissipated in the body, not the kinetic energy of the impacting object. For a review of literature on drone-like human injuries, see [21]. A number of reasonably accurate and empirically verified models have been developed. One model that fits well to a drone (chest) impact scenario is [22] which uses a lumped-mass thoracic model to develop a VC parameter, where V is thorax compression velocity and C is compression relative to chest depth. The VC parameter for a given impact maps well to injury severity.

The blunt criterion (BC) [23] is useful because it does map kinetic energy to injury severity. It is defined as

$$\mathrm{BC} = \ln \frac{E}{W^{1/3} T D} \,, \tag{4}$$

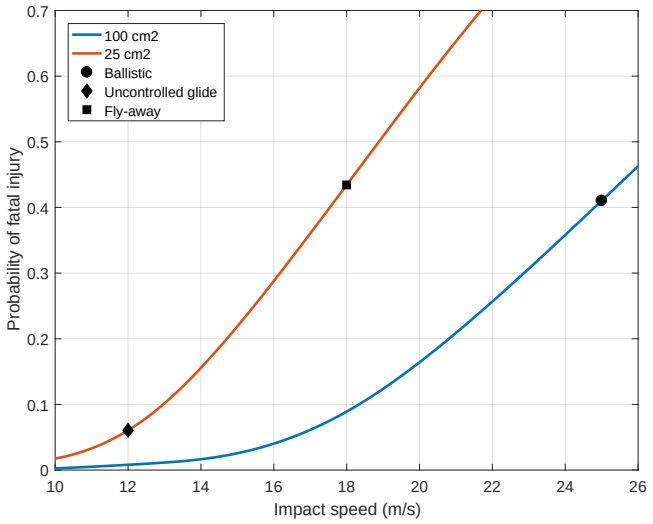

Fig. 3. Mapping from impact speed to probability of fatality for the Talon aircraft. Specifications for the aircraft and the simulated flight are found in Table I and II. The ballistic descent impact speed emerges from simulation and is approximately 25 m/s, and the fly-away impact speed is assumed equal to the cruise speed.

where E is kinetic energy, W is mass of impacted object, T is thickness of the body wall (in cm), and D is diameter of impacting object (in cm). According to [24] $T = kW^{1/3}$ with $k = 0.6$ for females and $k = 0.7$ for males, and according to [25] we have $\text{AIS} = 1.33 \cdot \text{BC} + 0.6$. And by interpolating the fatality rates normally associated with the AIS scale [26] we can now map kinetic energy to fatality rate. Note that an adaption of BC to impacts of drones is done in [27], where a generic drone design is used to develop formulas specifically for thorax and head impacts. It does not map all the way to fatality rate, though.

Figure 3 shows the map from impact speed to probability of fatality for the Talon aircraft. Since it for this mission operates at a fixed altitude and fixed cruise speed the graph does not change during the flight. The three relevant impact speeds can therefore easily be shown on the graphs.

III. RESULTS

The methods for quantifying the probability of fatality described in the previous section lends itself to a wide range of unmanned aircraft flight operations. It primarily requires knowledge on the aircraft specifications, a reasonably good population density map, a flight path, and assumptions on the probability of the flight terminating events. In the following the method is demonstrated in a given application where all the parameters are available. Subsequently, it seems reasonable to assume that the risk associated with flights with the same aircraft at other geographical locations has an equivalent level as long as these locations have parameters similar to the ones used for the computation done here.

A. Aircraft and flight path

To demonstrate the ability of the proposed method for estimating probability of fatality for a given flight we employ

Fig. 4. Talon modified model aircraft used by Heliscope.

TABLE I
TALON AIRCRAFT SPECIFICATIONS.

Flight time	1 h 15 min
Mass m	3.75 kg
Cruise speed	18 m/s
Glide speed	12 m/s
Glide ratio	$N(\mu = 12, \sigma = 2)$
Probability of ballistic descent	1/50 per hour
Probability of uncontrolled glide	1/50 per hour
Probability of fly-away	1/100 per hour
Drag coefficient at ballistic descent	$N(\mu = 0.9, \sigma = 0.2)$
Area for drag at ballistic descent	0.1 m^2
Area for person impact at ballistic descent	100 cm^2
Area for person impact at glide and fly-away	25 cm^2

the specifications of the Heliscope aircraft and an actual BVLOS flight demonstration conducted December 1, 2016. The aircraft is a modified Talon, shown in Figure 4. It is equipped with a down-looking camera for imagery of power lines for post flight inspection as well as a forward looking camera to aid the pilot during BVLOS flight and in emergency situations. It is powered by a single electric motor with push-propeller, and has additional LiPo battery capacity compared to the standard version. The autopilot is a PixHawk and the ground control station is a standard laptop running Mission Planner. The aircraft parameters used in the risk assessment computation are given in Table I.

The flight path is an approximately 16 km long almost straight stretch that follows a large power line. This is flown in both directions, with a 10 meter offset to the center of the power line, making the total flight about 33 km, including turn at the end and take-off and landing. A total of 95 waypoints (WP) are set along the power line, with an average distance of 350 meters in order to follow the bends of the power line as well as the varying terrain elevation. Except for take-off and landing the entire flight is flown at 80 m AGL and at cruise speed. The geographical location of this flight has been chosen because it is a (by Danish standards) less populated area, and the take-off location has easy access by road and features a larger field which the owner would let the project use. No other property owners along the flight

TABLE II

FLIGHT AND SIMULATION SPECIFICATIONS.

Flight distance	32.9 km
Flight time at cruise speed	$\sim$ 30 min
Flight speed (cruise speed)	18 m/s
Flight altitude	80 m AGL
Number of WPs	95
Wind speed	$N(\mu = 0, \sigma = 5)$
Wind direction	unif$(0, 2\pi)$
Person area A_{person}, ballistic descent	0.3 m^2/person
Person area A_{person}, glide and fly-away	0.6 m^2/person
Shelter factor S	0.3
Sample distance, ballistic descent	50 m
Sample distance, uncontrolled glide	200 m
Sample distance, fly-away	Every WP

path were informed of the flight.

The flight path is shown in Figure 5 along with (one version of) the population density map and some topographical information. This flight was conducted according to a special permit given by the Danish Transport, Construction and House Authority as part of the joint BVLOS FastTrack project and based on the results presented in this work. An excerpt from one of the images captured on the December 1 flight is shown in Figure 6.

B. Flight path sampling

The flight path is available as a set of WGS84 coordinates. For the purpose of computing probability of fatality during the flight the path is sampled at equidistant points (and more densely than the WPs) under the assumption that the flight path is straight lines between WPs. The sample density is chosen such as to match the geographical extend of the probable impact area for each of the three events described in Section II-B as well as the population density map appropriate for each event. As the size of the probable impact area for the ballistic event is in the order of 100 m by 100 m the sampling density for this event is set to 50 m. The population density map used is 25 m by 25 m. A more dense sampling of the flight path than this only gives negligibly different results. Similarly the sample density of the uncontrolled glide is set to 200 m. The sample density for a fly-away can be as high as several km, but for practicable purpose in the computation is set to each WP (averaging 350 m sample density). The wind is assumed to be uniformly distributed in direction and normally distributed in speed with 0 mean and standard deviation of 5 m/s. While the wind direction and speed is known for the December 1 flight the risk assessment will not assume specific prior knowledge of the wind conditions. The parameters used in the simulation is listed in Table II.

C. Computing probability of fatality

In the following the ballistic descent (BD) is used to describe the fatality probability computation, but the same procedure is used for uncontrolled glide and fly-away (and with the parameters pertaining to those two events).

For each sample point on the flight path the parameters for that point is used to determined the ground impact PDF relative to that point (see an example in Figure 2). Offsetting the PDF relative to the coordinates of the assumed event point gives the probability of the aircraft impacting the ground in absolute coordinates. The PDF matrix is then entry-wise multiplied with the population density map (appropriately sampled matrix $\mathbf{D}$) for the same area and the result is a map of the probability of impacting a person with the size of one pixel in the PDF map, that is a 1 m^2 large person. A summation over this map gives the probability of impacting a 1 m^2 person given a ballistic descent. We assume that a person takes up a particular area that depends on the expected impact angle, and this value is multiplied onto the result. Additionally, it is multiplied with the shelter factor S. This will then provide the probability $p_{\text{impact person}}$ of impacting a person (see (1) above) given a particular event at the given event point. The computation can be formulated as

$$p_{\text{impact person}} = S \cdot A_{\text{person}} \cdot \sum_{\substack{\text{latitude} \\ \text{longitude}}} \text{PDF} \circ \mathbf{D} \,, \qquad (5)$$

where $\circ$ is the Hadamard product and $\cdot$ is the scalar product.

For each sample point the probability of fatal injury $p_{\text{fatal impact}}$ can also be computed. This is done using the simulation and descent parameters as described in Section II-G, and this probability is used in (1) along with the event probability p_{event} to give the probability of fatality p_{fatality}. This probability is valid for the period of time where the aircraft is in the vicinity of the flight path sample point; for computational purposes we will assume that this probability is valid from the given event point until the next is reached. With the sample distances given in Table II the time between event points is about 3 seconds for ballistic descent, 11 seconds for uncontrolled glide, and 19 seconds for fly-away. The time-varying probabilities of fatality are shown in Figure 7. There are distinct differences between the three graphs. The ballistic descent is targeting a relatively small impact area with a comparatively high probability. At the same time the resolution of the population density map is small, and because the flight is over a thinly populated area many of the (small) cells in this map have zero density. Consequently, for many of the sampled event points along the flight path the crash area for the ballistic descent only covers zero density cells. And therefore this graphs is zero for most of the flight. And whenever the aircraft passes over a farm or cluster of houses, the probability increases briefly.

The uncontrolled glide impact area is somewhat larger (roughly two order of magnitudes) than that of the ballistic descent, and the population density map used is comparatively more coarse. As a consequences the probability of fatality graph is much more smooth. Once large peak is seen just prior to the aircraft reaching the point where it turns around and flies back along the same path. This is because the flight path ends just south of the city of Bjerringbro, and even though the aircraft turns around before overflying the

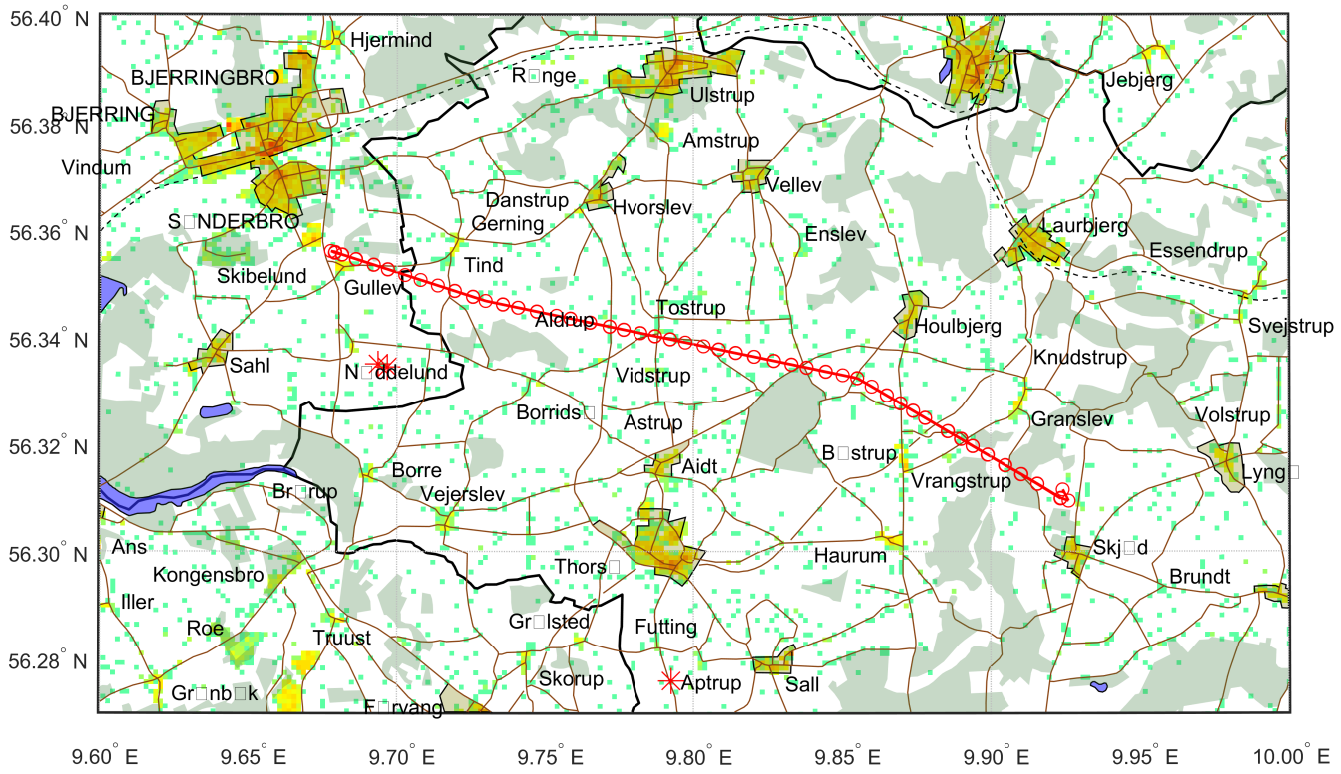

Fig. 5. Flight path for December 2016 test flight. The flight starts south of Granslev and goes up to south of Bjerringbro, where the aircraft makes a U-turn and flies back along the same set of WPs to the take-off location. Each red circle represents a waypoint. The background population density map is with 100 m resolution and is described in Section II-F. The topographical information is the same as in Figure 1. The red stars are wind turbines.

Fig. 6. Excerpt from a an image captured by the Talon aircraft onboard downlooking camera during the December 1 test flight.

city, in the event of an uncontrolled glide the aircraft would still be able to glide into the very southern part of the city. This can be seen on Figure 5. As soon as the aircraft has turned to fly back the probability drops.

The fly-away impact area is quite large, covering many square kilometers. Therefore it changes relatively little during the flight. The slow increase is an effect of the maximum flight range decreasing during the flight and the city of Aarhus (population ∼270.000) being within range of a fly-away for the entire flight. Therefore, this city constitutes an increasing part of the potential impact area as the flight progresses.

D. Joint probability of fatality

For each of the events the average probability of fatality is computed and summed to give the total probability for the entire flight. This is shown in Table III. Also, a series of intermediate results are available for this methods, including probability of impact a person (graphs similar to those in Figure 7, but obviously with higher probabilities) and number of people subjected to a potential drone crash. For these results only the totals are given, see Table III. It is important to note that the probabilities given in Table III are rather approximative for two reasons; 1) they are based on a series of assumptions that display varying degree of accuracy and obviously the end result is no more accurate than these assumptions (see Section III-E), and 2) the probabilities should have been conditional in the sense that the probability of an event at any give time is conditional on that any event has not yet occurred. For instance, a fly-away at a given time is conditional on the aircraft not experiencing a ballistic descent prior to this time. However, as all the probabilities are indeed relative small the error is negligible compared to the inaccuracy caused by previously mentioned assumptions.

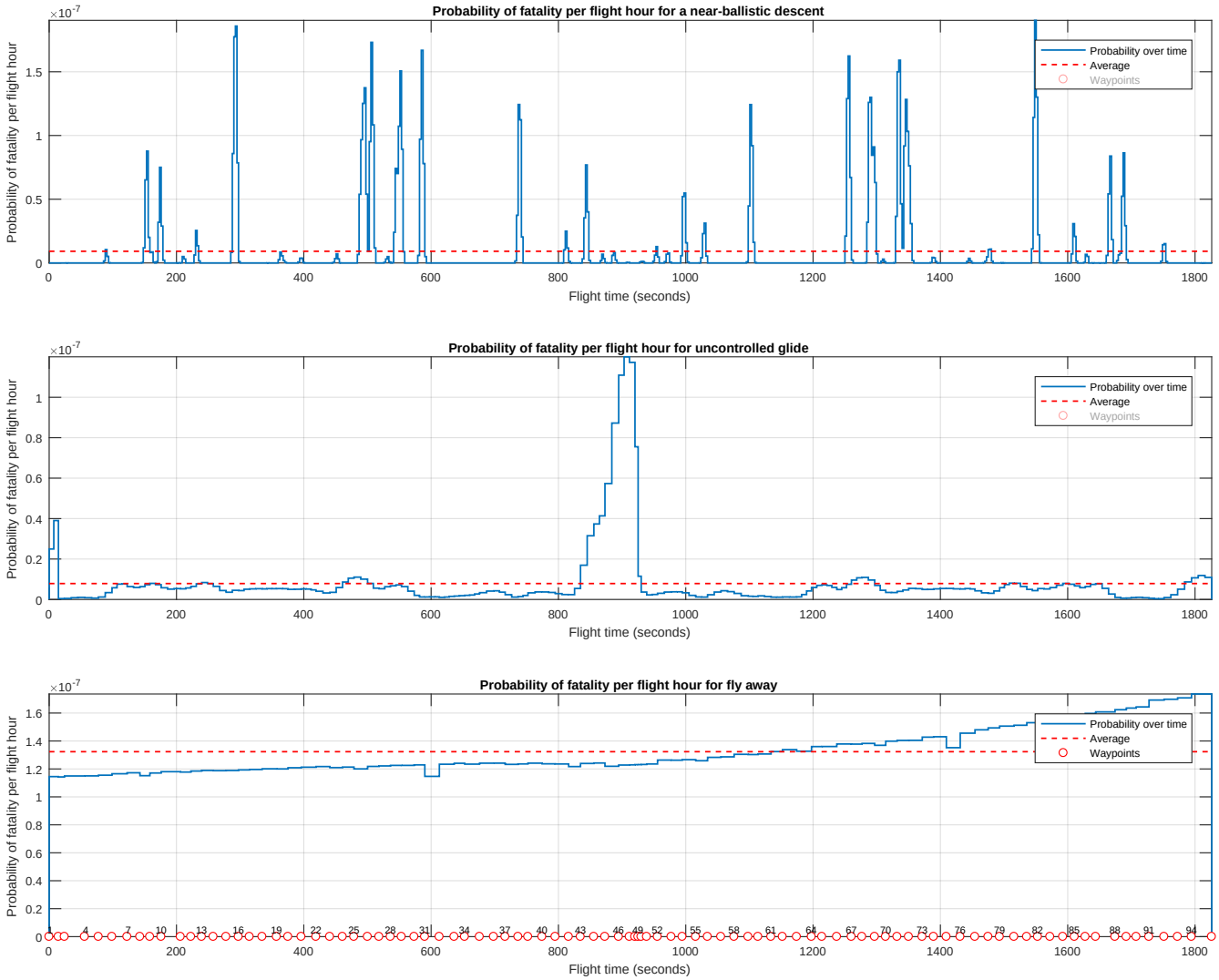

Fig. 7. The probability of fatality for the three event types as a function of time during the flight. The dashed red line shown the average for the entire flight. At the bottom of the third graph is shown the time location of the 95 waypoints.

TABLE III

PROBABILITIES OF PERSON IMPACT AND OF RESULTING FATALITIES.

	Ballistic	Uncontrolled glide	Fly away	Total
Person impact probability per flight hour	$2.2 \cdot 10^{-8}$	$1.3 \cdot 10^{-7}$	$3.0 \cdot 10^{-7}$	$4.6 \cdot 10^{-7}$
Average probability of fatality on impact	0.42	0.061	0.43	n/a
Fatality probability per flight hour	$9.2 \cdot 10^{-9}$	$7.9 \cdot 10^{-9}$	$1.3 \cdot 10^{-7}$	$1.5 \cdot 10^{-7}$

E. Interpretation and validity of results

The list of assumptions enabling the computation of the probabilities shown in Figure 7 and in Table III is fairly long and holds values that are estimates based on work done by others on other drones, some estimates are based on general knowledge about small unmanned aircraft, and some of the parameters are pure guesswork and remains unproven. It would be valuable to determine how these uncertainties affect the uncertainty of the results, but since some of the computations are rather nonlinear the effect of varying the parameters is not easy to determine. A study of the sensitivity of the individual parameters remains as future work.

The substantial uncertainty aside the estimated parameters in Table I and II have deliberately been chosen slightly conservative to reduce the risk that the derived probabilities are unrealistically low. Consequently, as it is indeed likely that estimate of 10^{-7} fatalities per flight hour is an order of magnitude wrong (in the sense that if this particular aircraft were to fly the specified mission repeatedly for 10^{7} hour, with suitable maintenance etc. we would on average see one fatality) it is still within the uncertainty range that applies to similar considerations for manned aviation.

IV. CONCLUSIONS

The method applied to the power line inspection flight demonstrates how it is possible to quantify an estimate of the probability of fatality for a specific flight. The computations are easy to repeat for another flight path, and indeed for another aircraft. It is important to note that the risk assessment here does not cover all possible flight terminating events, as does it not include midair collision. However, it is relatively easy to include additional events (which is certainly necessary for other aircraft types, such as rotorcraft), and the flight is conducted in such a fashion that midair collisions are highly unlikely. For approval of BVLOS flights this method contributes in a tangible way to assist the authorities in determining the risk associated with a given type of flight operations, and as indicated above the Danish Transport, Construction, and Housing Authority accepts this method as a valid tool to anyone applying for permit to conduct BVLOS operations in Danish airspace.

There remains lots of future work to improve and refine the method, as well as including more events, and more types of aircraft. Also, more accuracy on assumptions will be beneficial for the resulting probabilities.

ACKNOWLEDGMENT

This work is supported by the BVLOS FastTrack project between the Danish Tranport, Construction and Housing Authority, University of Southern Denmark, Aalborg University, UAS Test Center Denmark, and Heliscope. We wish to thank the partners for providing information and data for this work.

REFERENCES

[1] R. A. Clothier, B. P. Williams, and N. L. Fulton, "Structuring the safety case for unmanned aircraft system operations in non-segregated airspace," *Safety Science*, vol. 79, pp. 213–228, 2015. [Online]. Available: http://dx.doi.org/10.1016/j.ssci.2015.06.007

[2] R. A. Clothier and R. A. Walker, "The Safety Risk Management of Unmanned Aircraft Systems," in *Handbook of Unmanned Aerial Vehicles*, K. P. Valavanis and G. J. Vachtsevanos, Eds. Springer Science + Business Media B.V., Dordrecht, Netherlands, 2013, p. 37.

[3] X. Lin, N. L. Fulton, and M. E. T. Horn, "Quantification of high level safety criteria for civil unmanned aircraft systems," in *IEEE Aerospace Conference Proceedings*, no. September, 2014, p. 13.

[4] E. Denney, G. Pai, and I. Habli, "Perspectives on software safety case development for unmanned aircraft," *Proceedings of the International Conference on Dependable Systems and Networks*, 2012.

[5] E. Denney and G. Pai, "Architecting a Safety Case for UAS Flight Operations," in *34th International System Safety Conference*, 2016.

[6] D. W. King, A. Bertapelle, and C. Moses, "UAV Failure Rate Criteria for Equivalent Level of Safety," in *International Helicopter Safety Symposium*, Montreal, 2005, p. 9.

[7] P. Wu and R. Clothier, "The Development of Ground Impact Models for the Analysis of the Risks Associated with Unmanned Aircraft Operations Over Inhabited Areas," in *Proceedings of the 11th Probabilistic Safety Assessment and Management Conference (PSAM11) and the An- nual European Safety and Reliability Conference (ESREL 2012)*, 2012, p. 14.

[8] R. Clothier, R. Walker, N. Fulton, and D. Campbell, "A casualty risk analysis for unmanned aerial system (UAS) operations over inhabited areas," in *Second Australasian Unmanned Air Vehicle Conference*, 2007, pp. 1–15.

[9] R. Clothier, B. Williams, and A. Washington, "Development of a Template Safety Case for Unmanned Aircraft Operations Over Populous Areas," in *SAE 2015 AeroTech Congress & Exhibition*, sep 2015, p. 10. [Online]. Available: http://papers.sae.org/2015-01-2469/

[10] A. la Cour-Harbo and H. Schioler, "Ground impact probability distribution for small unmanned aircraft in ballistic descent," 2017, preprint. [Online]. Available: http://vbn.aau.dk/da/publications/ground-impact-probability-distribution-for-small-unmanned-aircraft-in-ballistic-descent(dc2d6dc0-30f4-44cd-a989-98962b925a76).html

[11] A. la Cour-Harbo, "Quantifying ground impact fatality rate for small unmanned aircraft," 2017, preprint. [Online]. Available: http://vbn.aau.dk/da/publications/quantifying-ground-impact-fatality-rate-for-small-unmanned-aircraft(bc811620-07b3-49c7-a86f-41f9a8dd409e).html

[12] P. Freeman and G. J. Balas, "Actuation failure modes and effects analysis for a small UAV," in *2014 American Control Conference*. IEEE, jun 2014, pp. 1292–1297.

[13] P. M. Freeman, "Reliability Assessment for Low-cost Unmanned Aerial Vehicles," Ph.D. dissertation, University of Minneota, 2014.

[14] Office of the Secretary of Defence, "Unmanned Aerial Vehicle Reliability Study," Department of Defense, Tech. Rep. February, 2003. [Online]. Available: http://www.acq.osd.mil/uas/docs/reliabilitystudy.pdf%5Cnfile://d/Technical/uavs/U market analysis/UAV reliabilitystudy.pdf

[15] S. Reimann, J. Amos, E. Bergquist, J. Cole, J. Phillips, and S. Shuster, "UAV for Reliability," AEM 4331 Aerospace Vehicle Design, Tech. Rep. December, 2013.

[16] ——, "UAV for Reliability Build," University of Minnesota, Tech. Rep., 2014.

[17] R. Venkataraman, "Reliability Assessment of Actuator Architectures for Unmanned Aircraft," Ph.D. dissertation, University of Minnesota, 2015.

[18] R. Venkataraman, M. Lukátsi, B. Vanek, and P. Seiler, "Reliability Assessment of Actuator Architectures for Unmanned Aircraft," *IFAC-PapersOnLine*, vol. 48, no. 21, pp. 398–403, 2015. [Online]. Available: http://linkinghub.elsevier.com/retrieve/pii/S2405896315016882

[19] J. F. Murtha, "An Evidence Theoretic Approach to Design of Reliable Low-Cost UAVs," Ph.D. dissertation, Virginia Polytechnic Institute, 2009.

[20] K. Dalamagkidis, K. P. Valavanis, and L. A. Piegl, "On unmanned aircraft systems issues, challenges and operational restrictions preventing integration into the National Airspace System," *Progress in Aerospace Sciences*, vol. 44, no. 7-8, pp. 503–519, 2008.

[21] A. la Cour-Harbo, "Mass threshold for 'harmless' drones," *International Journal of Micro Air Vehicles*, p. 11, 2017.

[22] D. C. Viano and I. V. Lau, "A viscous tolerance criterion for soft tissue injury assessment," *Journal of Biomechanics*, vol. 21, no. 5, pp. 387–399, 1988.

[23] V. R. Clare, A. P. Mickiewicz, J. H. Lewis, and L. M. Sturdiven, "Blunt Trauma Data Correlation," Report EB-TR-75016. Edgewood Arsenal, Tech. Rep. May, 1975.

[24] L. M. Sturdivan, D. C. Viano, and H. R. Champion, "Analysis of injury criteria to assess chest and abdominal injury risks in blunt and ballistic impacts." *The Journal of trauma*, vol. 56, no. 3, pp. 651–663, 2004.

[25] C. A. Bir and D. C. Viano, "Design and injury assessment criteria for blunt ballistic impacts," *The Journal of Trauma, Injury, Infection, and Critical Care*, vol. 57, no. December, pp. 1218–1224, 2004.

[26] AAAM, "Abbreviated Injury Scale (AIS) 2005 Manual," Association for the Advancement of Automotive Medicine, Tech. Rep., 2005.

[27] A. Radi, "Human injury model for small unmanned aircraft impacts," Civil Aviation Safety Authority, Australia, Tech. Rep., 2013.